Material Grain Size Determines Relaxation-Time Distributions in Slow-Dynamics Experiments

Material Grain Size Determines Relaxation-Time Distributions in Slow-Dynamics Experiments

J. Kober,[1,2] A.S. Gliozzi,[2] M. Scalerandi,[2,*] and M. Tortello[2]

[1] *Institute of Thermomechanics, Czech Academy of Sciences, Prague, Czech Republic*

[2] *Department of Applied Science and Technology (DISAT), Politecnico di Torino, Torino, Italy*

(Received 8 February 2021; revised 15 November 2021; accepted 23 November 2021; published 3 January 2022)

By measuring the elastic slow dynamics behavior of various consolidated granular materials and metallic alloys, we show that the evolution of the wave velocity as a function of time can be reproduced by using a continuous relaxation-time spectrum, whose main features can be extracted from the experiments. Here we propose to adopt a Weibull distribution of the relaxation times, that we find to display a maximum, which is related to the material grain size and independent of the conditioning amplitude. These results show that the role of the grain-size distribution is fundamental to quantify slow dynamics effects, as well as to clarify its mesoscopic physical origin. Moreover, they can pave the way for the implementation of advanced characterization methods or nondestructive testing techniques capable of retrieving information on the different spatial scales or defects in the materials under investigation.

DOI: 10.1103/PhysRevApplied.17.014002

I. INTRODUCTION

Slow relaxation phenomena that do not follow a typical exponential behavior take place in diverse physical systems [1–3]. In some cases, suitable relaxation curves have been introduced to describe their behavior [1,4], but, usually, they are described in terms of the combination of exponential relaxation processes with different time rates [5–7]. The existence of a broad relaxation-times spectrum could be correlated to the spatial scales present in the physical system, e.g., pore radii [5] or grain sizes [8].

Slow dynamics is a relaxation phenomenon in hysteretic elastic solids. It can occur both during conditioning and relaxation. The former is described as the variation, in time, of the elastic wave-propagation velocity and attenuation, when an excitation at a given strain level is applied [9]. Relaxation occurs when the excitation is removed: velocity and damping recover, slowly in time, to their original equilibrium value [10,11]. These effects have been observed in rocks [12], consolidated [13–15] and unconsolidated [16] granular media, damaged composites, polymers and polycrystalline metals [17,18]. Slow dynamics phenomena arise from the coexistence of multiple equilibrium states, defined by different values of the viscoelastic properties (modulus and damping) at different amplitudes of the strain applied to the material [19–22].

The possibility of further understanding the mechanisms that produce the time evolution of the viscoelastic properties of the material during the relaxation process, plays a crucial role in identifying its underlying physical mechanisms, which can be redistribution of fluids [23,24], sliding, adhesion and/or friction [25], rearrangement of dislocations [26], or clapping surfaces [27], etc.

A possible approach to the problem is to interpret the relaxation process as a multirelaxation phenomenon, by fitting experimental curves with a superposition of time-decaying exponentials. Shokoui *et al.* applied this approach by using a finite, discrete basis of exponentials [7]. Snieder proposed a continuous relaxation spectrum proportional to $1/\tau$ by fixing minimum and maximum bounds to the range of possible relaxation times [28]. Both approaches have some limitations in view of establishing correlations with the material spatial scales and properties. Moreover, they represent two limiting conditions of a more general approach, that we present here.

In a more general way, the problem is that of determining a "physically reasonable," continuous distribution function describing the relaxation-time spectra starting from experimental data, and obtaining the parameters of a function that allows to fit the data. Two main issues, however, make the procedure complex: (i) relaxation times span over 5–6 decades, since both short and long times play a role in the slow dynamics recovery and (ii) due to the presence of noise and experimental limitations to access all time scales, the problem is not well posed. As a consequence, the distribution function describing the phenomenon might not be unique [2].

Here, we show that it is possible to determine, starting from data acquired from different materials under an elastic excitation, a reasonable and physically grounded solution,

*marco.scalerandi@polito.it

and that some characteristic features of the obtained distributions, like the peak position, are directly related to the material properties like the grain size, and independent of amplitude of the conditioning strain.

II. MATERIALS AND METHODS

A. Materials

Several samples with different grain structures are considered. Specifically, we analyze the following:

(a) Civil engineering concrete (sample Conc-B06): in the shape of a cylinder (40 mm diameter and 160 mm length). It is drilled from a casting prepared with 340 kg of cement (CEM II A-L 42.5 R), 957 kg of sand (0–5 mm), 846 kg of gravel (5–15 mm), and 200 kg of water (w/c ratio 0.59).

(b) Mortar (sample Mort-P23): in the shape of a prism ($40 \times 40 \times 160$ mm^3), produced using Portland cement. Sand grains are about 500 μm size.

(c) Berea sandstone (sample Ber-BE9): in the shape of a thin cylinder (10 mm diameter and 250 mm length). The size of the grains in this sample is of the order of 150 μm and the sample is very homogeneous.

(d) Low-quality concrete (Conc-X04): in the shape of a prism ($30 \times 30 \times 130$ mm^3), produced with proportions of two volumes of cement, four volumes of sand, and six volumes of gravel per volume of water (the average gravel size is 5 ± 2 mm);

(e) 3D-printed titanium alloy (sample TiAl-3DA): in the shape of a prism ($100 \times 20 \times 15$ mm^3), produced by SEBM using an Arcam Q20+ system and Ti-6Al-4V powder of particles of 45 to 105 μm diameter. Two typical size scales are present: the grain structure of the alloy is of the order of 40 μm and the space scale of about 1 mm of the layered structure, which is induced by the production procedure.

(f) Aluminum alloy D16CT1 equivalent to 2024 Al-4Cu-1Mg (sample Alu-C20): in the shape of a prism ($100 \times 20 \times 20$ mm^3) with the standard properties of aluminum alloy and grain sizes of the order of 350 μm.

Table I summarizes the samples type, name, and typical grain size.

TABLE I. Type, name, and estimated average grain size of the investigated materials. See also Refs. [29–31].

Material	Name	Mean grain size
Concrete	Conc-B06	10 mm
Mortar	Mort-P23	0.5 mm
Berea Sandstone	Ber-BE9	0.15 mm
Concrete	Conc-X04	5 mm
Ti-6Al-4V	TiAl-3DA	0.04 mm and 1 mm
Al alloy	Alu-C20	0.35 mm

B. Experimental setup

Ultrasonic input signals are excited by an Agilent 33500 arbitrary waveform generator, amplified 20 times, and sent to a Matest C370-02 (resonance frequency approximately equal to 55 kHz) or IMG (resonance frequency approximately equal to 27 kHz) piezoelectric transducer glued to the basis of the sample by means of phenyl salicylate or cyanoacrylate glue. A Matest C370-02 transducer is placed at the other end of the sample to record output signals using an Agilent-Infiniuum DSO9024H or Picoscope 6402C oscilloscope.

To ensure that the obtained results are not dependent on the specific arrangement of the sample position and orientation, two different configurations are used. In the first, the samples (Ber-BE9, Mort-P23, TiAl-3DA) are vertically suspended and enclosed in a styrofoam box to reduce ambient thermal drifts. In the second arrangement, the samples (Ber-BE9, Conc-B06, Conc-X04, and Alu-C20) are placed horizontally on a soft foam support. Conc-B06 is tested inside a climate chamber at constant temperature and relative humidity.

The measurement procedure to monitor the relaxation process is implemented following two complementary protocols:

(a) Protocol I (Mort-P23, Ber-BE9, Conc-X04, and Conc-B06 samples). The sample is excited by a continuous wave at low amplitude and frequency close to the resonance mode (preconditioning phase). During preconditioning the amplitude is kept small to avoid any nonlinear effect. Sinusoidal signals $u_p(t)$ are detected, repeating many times the same acquisition. The amplitude of the sinusoidal excitation is increased to induce conditioning (this phase is not monitored here). Duration of conditioning is in the range of 5 min. Afterwards, the input amplitude is reduced again to the low linear value and monitoring of relaxation starts, acquiring again successive sinusoidal signals $u_r(t)$.

(b) Protocol II (Ber-BE9, TiAl-3DA, Alu-C20 samples). The procedure is very similar except that, during preconditioning and relaxation, the input source is a low-amplitude chirp of duration 30 ms with frequency linearly varying in a narrow range around the first longitudinal mode. The chirp excitation is repeated in defined intervals during preconditioning and relaxation. Conditioning is induced using a sinusoidal wave as in protocol I. The duration of the chirp was defined after verifying that the use of longer chirps is not affecting the results of the analysis [32].

The frequency ranges used to test the various samples are reported in Table II.

TABLE II. Frequency ranges used to test the various samples.

Material	Monochromatic wave testing	Sweep wave testing
Conc-B06	12.8 kHz	
Mort-P23	22.7 kHz	
Conc-X04	22.5 kHz	
Ber-BE9	17.2 kHz	8.1–11.1 kHz
TiAl-3DA		23.1–28.1 kHz
Ali-C20		18.4–21.4 kHz

The experiments are performed by varying the conditioning amplitude from a very small value (estimated strain during preconditioning of the order of 10^{-7}) to larger strain amplitudes (from 10^{-6} up to 10^{-5} during conditioning). Strains are estimated using the protocol reported in Ref. [33]. In both protocols, the relaxation is monitored for no longer than 500–1000 s, which allows us to perform a full set of conditioning amplitudes within 2 h. The longitudinal propagation velocity as a function of time is derived by using the method "MoDaNE," described in Ref. [34] and summarized in the next subsection.

The two protocols have complementary advantages: the first one is very fast, and allows an easier detection of the early times of the relaxation process; protocol II is slower but very accurate, making it possible to observe very small changes in velocity, such as those exhibited by metal alloys.

C. Data analysis

In both protocols described above, the propagation velocity is derived using a semianalytical formulation (MoDaNE) described in Ref. [34]. In protocol I, amplitude A and phase ϕ of each detected signal are used to determine the velocity c by an inversion of the theoretical solution of the problem. Each signal is acquired at a defined detection time, thus the behavior of velocity as a function of time is obtained.

For a sample of length L, defining ω as the angular frequency, and k as the wave number, we have

$$c(t) = \omega/k = \frac{\omega}{\frac{1}{L}\left(\pi n \pm \arctan\sqrt{\frac{z}{2\cos^2(\phi)}}\right)}, \tag{1}$$

where the sign is plus if $\phi + \phi_0 > 0$, n is the order of the closest mode to ω and

$$z = -(U_0)^2 - \cos(2\phi) + \sqrt{1 + (U_0)^4 + 2\cos(2\phi)(U_0)^2}. \tag{2}$$

Here U_0 and ϕ_0 are the properly calibrated amplitude and phases of the source function.

In protocol II, we take advantage directly of the theoretical expression for the analytical solution of the displacement in $x = L$. We have the following dependence of amplitude on frequency [9]:

$$A = \frac{U_0}{\sqrt{\cosh^2(\alpha L) - \cos^2(kL)}}. \tag{3}$$

For each measured signal a discrete-time Fourier transform is calculated and the velocity is determined by fitting Eq. (3) to the spectrum.

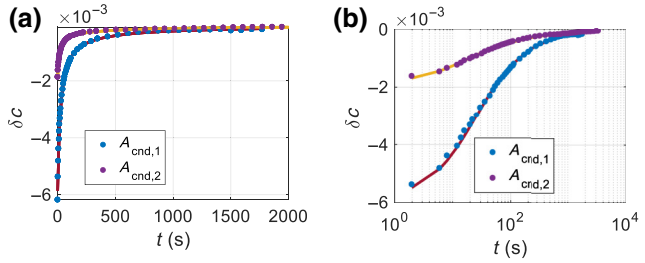

FIG. 1. Evolution of the relative velocity variation in the sample Conc-B06, during the relaxation process for two different conditioning amplitudes. (a) Linear time scale. (b) Logarithmic time scale.

D. Experimental results

A typical observed behavior of the relative velocity variation during relaxation is shown, for the sample Conc-B06, as symbols, in Fig. 1 in a linear (a), and logarithmic (b), time scale, for two conditioning amplitudes. Here,

$$\delta c(t) = [c(t) - c_{\text{pre}}]/c_{\text{pre}} \tag{4}$$

is the relative variation of velocity c at time t with respect to the velocity c_{pre} measured in the preconditioning phase.

By looking at (b), we notice that, immediately after conditioning, the velocity assumes a starting value smaller than the preconditioning value and after an initial recovery, in the intermediate time range, it evolves logarithmically with time. Finally, it relaxes back to the original value.

The case reported in Fig. 1 refers to the concrete sample (Conc-B06), which shows the highest roll-off time t_r [corresponding to the onset of the $\log(t)$ behavior]. Data for other samples show a much smaller roll-off time, comparable with those reported in the literature. t_r in rocks was reported to range from about 10 ms (sandstone) to almost 1 s (soapstone) [7], but roll-off times of up to more than 20 s were observed in granite for civil-engineering applications [35].

Finally, we recall that the definition of the relaxation-time origin $t = 0$ is nontrivial since, during reverberation of the conditioning wave, relaxation and further conditioning might be superimposed. In our approach, we control time from electronics and define $t = 0$ as the time corresponding to the switching off of the conditioning amplitude. The reverberation time is analyzed along with the

time-measurement error. The total possible time shift is in the order of tens of milliseconds, which is shown not to affect the analysis of the data [32].

III. MULTIRELAXATION PROCESS

The process is an anomalous, nonexponential relaxation process and could be considered as a multirelaxation, i.e., a superposition of exponential (Arrhenius-like) decays with relaxation times τ:

$$\delta c(t) = \int_0^\infty F(\tau) e^{-t/\tau} d\tau, \tag{5}$$

where the function $F(\tau)$ is the relaxation-time spectrum. As mentioned previously, attempts have been reported in the literature to characterize the function $F(\tau)$ [7,28]. In both cases, the interpretation of the resulting relaxation-times spectra was not straightforward. We propose here a different approach to the solution, which consists in demonstrating that the distribution of relaxation times is continuous, significantly nonzero in a bounded range of τ values and presents a maximum.

To derive the main properties of $F(\tau)$ from the experimental data, we start by approximating the solution as a sum of exponentials with different weights. A basis of relaxation times must be defined. Since it must span a huge time interval, it is more practical to work in a logarithmic space [36]. The basis is a vector, $B = \{B_1, B_2, \ldots B_N\}$, where $B_i = \log_{10}(\tau_i)$. The elements are equally spaced, $\Delta_B = (B_N - B_1)/(N-1)$, and different bases can be chosen, by varying their dimension, N, or the upper and lower limits, B_1 and B_N. It follows

$$\delta c = \sum_{i=1}^{N} G_i e^{-t/10^{B_i}}, \tag{6}$$

where the coefficients G_i can be derived by fitting the experimental data. The results obtained are reported as yellow symbols in Fig. 2(a), for $N = 7$, $B_1 = -2$, and $\Delta_B = 1$. This approach is equivalent to that of Ref. [7].

The fitting procedure can be repeated K times, by changing the starting point of the basis $B_1 = B_1 + j/(K-1) * \Delta_B$ with $j = 0, 1, \ldots, K-1$. Blue symbols in Fig. 2(a) are the results obtained for sample Conc-B06 for $K = 30$. A continuous distribution, $G(B)$ is found, and thus

$$\delta c = \int_{B_{\min}}^{B_{\max}} G(B) e^{-t/10^B} dB. \tag{7}$$

To determine the continuous relaxation-times spectrum $F(\tau)$ in Eq. (5), one more step is necessary. Since $B = \log(\tau)$ and $dB = d(\log\tau) = d\tau/(\tau \ln 10)$, it follows

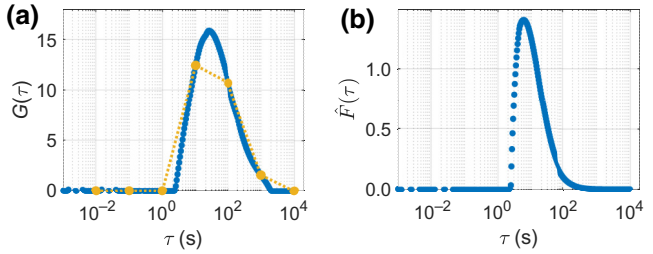

FIG. 2. (a) Discrete distribution, $G(\tau)$ in the logarithmic time scale obtained by using a basis of seven exponentials (yellow symbols). Repeating the fitting by shifting the B_1 (initial value for the basis), we obtain a continuous distribution (blue symbols). (b) Estimation of the distribution $\hat{F}(\tau)$ in the linear time scale, inferred from $G(\tau)$.

that

$$\delta c = \int_{B_1}^{B_N} \frac{G(B)}{\tau \ln 10} e^{-t/\tau} d\tau \tag{8}$$

and

$$\hat{F}(\tau) = G(B)/(\tau \ln 10), \tag{9}$$

where we introduce a first estimate of the distribution $F(\tau)$, named here $\hat{F}(\tau)$. The resulting distribution $\hat{F}(\tau)$ for the Conc-B06 sample is shown in Fig. 2(b).

Some comments should be made: (i) small errors in the calculation of the distribution $G(B)$ are amplified by the division by τ, especially for small relaxation times; (ii) an equal spacing when fitting in the logarithmic τ space [Eq. (6)], implies asymmetric steps in the integration of Eq. (9) in the linear space, that is, the τ values are no longer centered in the corresponding integration step. A correspondence between τ values defined in the logarithmic space and in the linear space is not straightforward, resulting in a shift of the position of the peak induced by the procedure (see the Supplemental Material [32]); (iii) the nonuniqueness of the solution and the sensitivity to the incompleteness of the data set is a known problem, intrinsic to the procedure.

Based on the above considerations, we can conclude that $\hat{F}(\tau)$ is not yet a reliable solution. Nevertheless, it allows us to draw indications about the general behavior of the solution. We note that the obtained distribution could be roughly approximated with a function of the form $F(\tau) = 1/\tau$ for a suitable interval of relaxation times, $\tau_{\min} < \tau < \tau_{\max}$, and equal to zero elsewhere, as in Ref. [28]. However, our findings allow us to go further. The analysis performed for all samples always suggests a similar shape of the distribution, which converges to zero for small and large τ values, peaked and asymmetric, with a faster increase at smaller τ values.

These indications can be used for identifying different choices for $F(\tau)$ that satisfy the above-mentioned

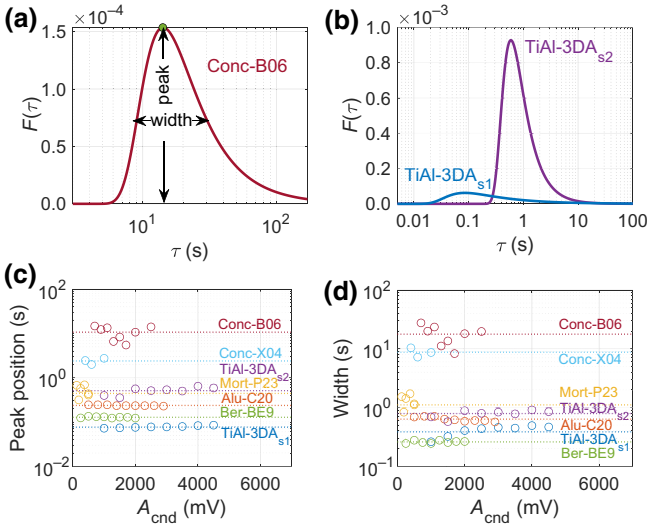

FIG. 3. (a) Continuous distribution function obtained by fitting with Eqs. (5) and (10) the measurements on Conc-B06 reported in Fig. 1. (b) Same as in (a) but for TiAl-3DA and by using a double-peaked distribution. Peak position, (c) and width at half maximum, (d) as a function of conditioning amplitude for the different materials.

properties. However, as shown within the Supplemental Material [32], despite differences in their shape, all of them share some relevant features, like the peak position, and thus are equivalent for the purposes of the present paper. We adopt here a Weibull distribution of the inverse of the relaxation times, since it is usually used to describe the distribution of the typical features at the length scale of grains or cracks [37,38]. Thus, defining $x = 1/\tau$ we write

$$F(\tau) = \beta \frac{\gamma}{\alpha}(x/\alpha)^{\gamma-1} e^{-(x/\alpha)^{\gamma}}. \tag{10}$$

An exception is represented by the TiAl-3DA sample, where a distribution with two asymmetric peaks is found, and the relaxation-time spectrum is thus the superposition of two Weibull distributions: $F(\tau) = F_{s1}(\tau) + F_{s2}(\tau)$.

The parameters of the distributions are obtained by fitting the curve $\delta c(t)$ in the linear time scale by integrating in the full τ domain using Eq. (5). A typical result, obtained on the sample Conc-B06, is shown in Fig. 1 for two different conditioning amplitudes (solid lines). The resulting fit is excellent and analogous quality is obtained for all other samples. The obtained distribution is reported in Fig. 3(a). Figure 3(b) shows the two Weibull distributions for the TiAl-3DA sample, which, combined, define $F(\tau)$.

IV. RESULTS AND DISCUSSION

The procedure is applied to analyze the relaxation data for the different materials under investigation. Two main parameters of the distributions are then considered as an indicator of the slow dynamics properties of a sample, as shown in Fig. 3(a): the peak position and the width at half maximum. The two parameters are obtained for different conditioning amplitudes A_{cnd}, by repeating the experiments at decreasing driving voltage of the generator during the conditioning phase. The conditioning amplitudes are chosen to have similar output amplitudes, i.e., comparable strain values for all samples [39].

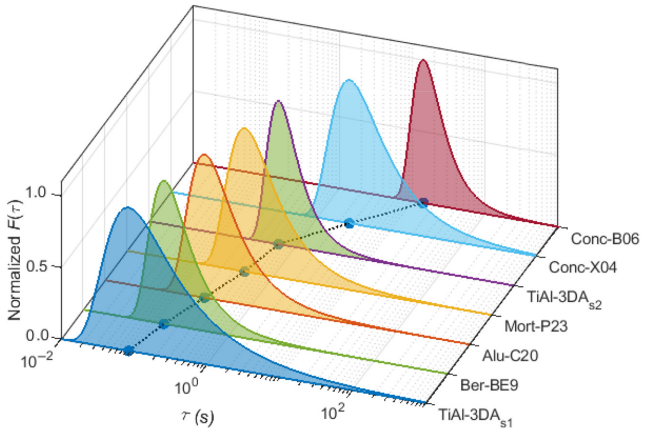

FIG. 4. Normalized representative distributions of all the investigated materials, plotted as a function of increasing peak position. The dashed line connects the projection of the peak positions on the zero-amplitude plane.

The obtained results, reported in Figs. 3(c) and 3(d) for the peak position and width, respectively, show that they are independent of A_{cnd}. Figure 4 reports the normalized distributions of all the investigated materials, ordering materials on the basis of their grain size. A clear shift of the peak position towards higher values is evident.

The properties of the distribution turn out to be correlated with the geometric features of the grains, as observed in Fig. 5, which reports the peak position as a function of the mean grain size. Particularly meaningful is the case of the TiAl-3DA sample: the two distinct peaks in the distribution function can be related to the two typical characteristic length scales that are found in this sample.

There is a close relationship between the characteristic relaxation times of the materials and one of their typical spatial scales (here, the grain size), in analogy to other physical systems [40], where a proportionality between relaxation times and correlation length has been observed. Moreover, the independence of the distribution parameters on the conditioning amplitude, shown in Figs. 3(c) and 3(d), indicates that the features, or "defects," that are responsible for the observed nonlinear effects are equally active at all tested conditioning amplitudes, regardless of their size.

The other parameter that turned out to be independent of the conditioning amplitude is the width of the distribution function, which, therefore, could also be related to some intrinsic property of the materials. Intuitively, one would expect that it is directly proportional

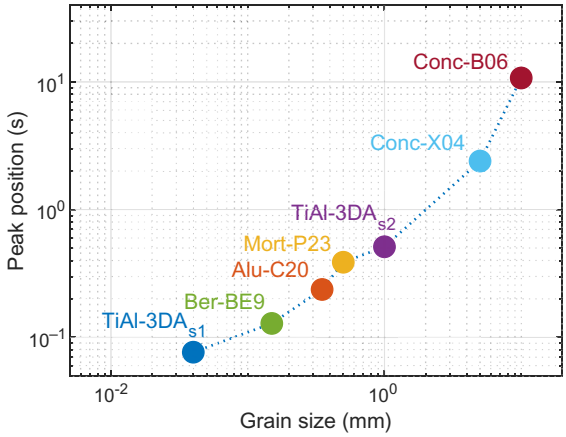

FIG. 5. Peak positions of the relaxation-time spectra for the different materials as a function of their mean grain size.

to the width of the distribution of grain sizes in the material, i.e., the dispersion around the average size. A qualitative inspection on some samples seems to support this hypothesis, which would however require, to be proved, a thorough and deep analysis that goes beyond the scope of the present paper and will be the subject of a future study.

The samples considered differ not only in the typical grain size, but also in other properties, e.g., damping, density, stiffness, sample size, etc. For trying to disentangle the correlation of different effects we consider experiments where some properties are changed while keeping the microstructure fixed. We test an aluminum sample with intact and weakened grain boundaries [Fig. 6(a)] and a concrete sample in different relative humidity conditions [Fig. 6(b)]. In all cases, the position of the peak remains unchanged, confirming our conclusions that the most probable relaxation time correlates to the grain size and dominant spatial scale only.

The use of chirp excitation signals combined with an accurate fit of the resonance curves allows extremely small variations of velocity to be measured with great accuracy (of the order of those observed by diffuse ultrasound [42]), but with the advantage that the wavelength of the signals does not need to be comparable to the scatterer size. In this way it is therefore possible to work at lower frequencies, for example, around the first longitudinal mode, generally allowing higher strain levels to be reached.

The possibility of quantifying the slow dynamics behavior by using features in the relaxation-time distribution—like the peak position, determined by the material grain size—that are independent from the conditioning amplitude, allows results that are independent from the conditioning strain to be obtained (see Fig. 3). This fact can be extremely relevant for applications because it does not require calibration of the strain [33] when the responses from different materials (or different frequencies) have to be compared.

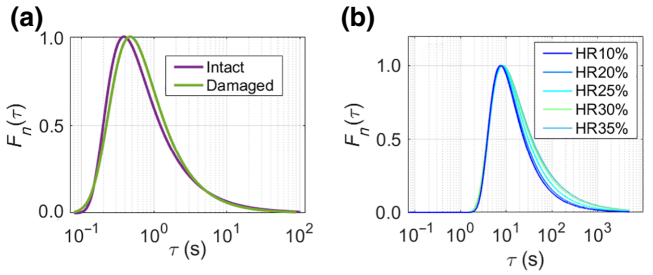

FIG. 6. Normalized relaxation-time distribution for (a) the aluminum sample tested in its intact state and after being damaged by the action of gallium, which modifies grain boundaries [41] and (b) the concrete sample tested in different relative humidity conditions.

The determination of the most relevant relaxation-time through relaxation measurements allows information about the relevant spatial scales of the material to be gained. In this regard, having proven the capacity of the method to resolve, at least to a certain extent, the concomitant presence of multiple spatial scales [see, for example, the results for the titanium alloy sample reported in Fig. 3(b)], the approach proposed here could be applied for determining the presence of microscopic features with a different spatial scale from that of the grains. This is, for example, the case of microcracks. Indeed, while the sensitivity of the nonlinear elastic parameters to the crack size is well known [43,44], the nonlinear response of the cracked samples is often difficult to separate from the nonlinearity of the intact specimen or from that due to the experimental setup. Thanks to our approach, in a characterization process, a splitting in the distribution of the relaxation times due to the presence of cracks with a typical spatial scale could represent a distinctive feature of the presence of damage and/or defects in the sample.

As a last consideration, we mention that linear [45], diffuse [46,47], and nonlinear [48] ultrasounds are often used to monitor physical processes and/or manufacturing procedures, during which microstructural changes are expected to take place. The sensitivity of slow dynamics to the microstructure spatial scale allows us to consider it as an indicator for monitoring slowly evolving processes, such as phase transitions, damage progression, curing, etc.

V. CONCLUSIONS AND PERSPECTIVES

Here we show that slow dynamics in elastic materials and, specifically, the relaxation of the elastic wave velocity could be described as a multirelaxation phenomenon, i.e., a superposition of an infinite number of Arrhenius-like relaxation effects, with a distribution of relaxation times derived directly from the experimental data. Such a distribution is significantly different from zero in a wide interval of relaxation times, peaked, and asymmetric.

A connection between the most relevant relaxation time (corresponding to the peak of the distribution) and the

grain size is demonstrated for materials with grain sizes ranging over 2 orders of magnitude. These observations are thus quite robust and could be possibly extrapolated to materials with smaller and larger grain sizes as well. Our results show that the grain size is one of the parameters controlling conditioning and relaxation, in both metal alloys and consolidated granular media. This fact could have interesting implications in the debate, still ongoing, over the physical origin of slow dynamics. Indeed, the observed correlation seems to indicate that the relevant physical phenomena could be confined to the grain surface rather than to the intergrain region, i.e., the volume of material filling the space between the grains. This could explain why a similar behavior is seen both in metals and rocks or consolidated granular media that feature very different intergrain regions. Moreover, the surface is the region where several phenomena can occur like, for instance, dislocation nucleation in metals, fluids redistribution in concrete, variations in the density of close contacts in dry granular media or crack surfaces. Thus, the correlation of the relaxation behavior with the grain size might support the hypothesis that one or more of these mechanisms are related to the origin of elastic hysteresis and conditioning in different classes of materials, also suggesting the direction of future investigations and experiments.

Applications of this approach are possible in several fields like, for instance, in materials characterization, process monitoring as well as in nondestructive testing. Indeed, the method proposed here allows ultrasonic wave velocity to be accurately measured and its small variations to be monitored over time with an excellent time resolution (of the order of a few milliseconds). Furthermore, the nonlinear effects caused by slow dynamics are measured here by using a linear method, i.e., by using a low-amplitude excitation signal, which simplifies considerably the experimental procedure [49,50]. This approach will likely turn out to be competitive with respect to other ultrasonic based techniques used to detect variations in materials microstructure. Work is ongoing in this regard [51].

ACKNOWLEDGMENTS

J.K. acknowledges support from the Grant Agency of the Czech Republic (GA19-14237S) and institutional support RVO: 61388998.

[1] P. Ilg, Equilibrium magnetization and magnetization relaxation of multicore magnetic nanoparticles, Phys. Rev. B **95**, 214427 (2017).

[2] K. Niss, J. C. Dyre, and T. Hecksher, Long-time structural relaxation of glass-forming liquids: Simple or stretched exponential?, J. Chem. Phys. **152**, 041103 (2020).

[3] R. A. Guyer, J. Ten Cate, and P. Johnson, Hysteresis and the Dynamic Elasticity of Consolidated Granular Materials, Phys. Rev. Lett. **82**, 3280 (1999).

[4] L. Ostrovsky, A. Lebedev, J. Riviere, P. Shokouhi, C. Wu, M. A. Stuber Geesey, and P. A. Johnson, Long-time relaxation induced by dynamic forcing in geomaterials, J. Geophys. Res. Solid Earth **124**, 5003 (2019).

[5] M. Kraft, J. Meissner, and J. Kaschta, Linear viscoelastic characterization of polymer melts with long relaxation times, Macromolecules **32**, 751 (1999).

[6] M. Tong, L. Li, W. Wang, and Y. Jiang, Determining capillary-pressure curve, pore-size distribution, and permeability from induced polarization of shaley sand, Geophysics **71**, A19 (2006).

[7] P. Shokouhi, J. Rivière, R. A. Guyer, and P. A. Johnson, Slow dynamics of consolidated granular systems: Multi-scale relaxation, Appl. Phys. Lett. **111**, 251604 (2017).

[8] A. Tarasov and K. Titov, Relaxation time distribution from time domain induced polarization measurements, Geophys. J. Int. **170**, 31 (2007).

[9] M. Scalerandi, C. Mechri, M. Bentahar, A. Di Bella, A. S. Gliozzi, and M. Tortello, Experimental Evidence of Correlations Between Conditioning and Relaxation in Hysteretic Elastic Media, Phys. Rev. Appl. **12**, 044002 (2019).

[10] M. Lott, M. C. Remillieux, V. Garnier, P. Y. Le Bas, T. J. Ulrich, and C. Payan, Nonlinear elasticity in rocks: A comprehensive three-dimensional description, Phys. Rev. Mater. **1**, 023603 (2017).

[11] M. C. Remillieux, R. A. Guyer, C. Payan, and T. J. Ulrich, Decoupling Nonclassical Nonlinear Behavior of Elastic Wave Types, Phys. Rev. Lett. **116**, 115501 (2016).

[12] J. Rivière, P. Shokouhi, R. A. Guyer, and P. A. Johnson, A set of measures for the systematic classification of the nonlinear elastic behavior of disparate rocks, J. Geophys. Res. Solid Earth **120**, 1587 (2015).

[13] J. Chen, J.-Y. Kim, K. E. Kurtis, and L. J. Jacobs, Theoretical and experimental study of the nonlinear resonance vibration of cementitious materials with an application to damage characterization, J. Acoust. Soc. Am. **130**, 2728 (2011).

[14] A. S. Gliozzi, M. Scalerandi, G. Anglani, P. Antonaci, and L. Salini, Correlation of elastic and mechanical properties of consolidated granular media during microstructure evolution induced by damage and repair, Phys. Rev. Mater. **2**, 013601 (2018).

[15] M. Scalerandi, M. Griffa, P. Antonaci, M. Wyrzykowski, and P. Lura, Nonlinear elastic response of thermally damaged consolidated granular media, J. Appl. Phys. **113**, 154902 (2013).

[16] V. Y. Zaitsev, V.E. Gusev, V. Tournat, and P. Richard, Slow Relaxation and Aging Phenomena at the Nanoscale in Granular Materials, Phys. Rev. Lett. **112**, 108302 (2014).

[17] C. Mechri, M. Scalerandi, and M. Bentahar, Enhancement of harmonics generation in hysteretic elastic media induced by conditioning, Commun. Nonlinear Sci. Numer. Simul. **45**, 117 (2017).

[18] J. Y. Yoritomo and R. L. Weaver, Slow dynamic elastic recovery in unconsolidated metal structures, Phys. Rev. E **101**, 012901 (2020).

[19] J. A. TenCate, E. Smith, and R. A. Guyer, Universal Slow Dynamics in Granular Solids, Phys. Rev. Lett. **85**, 1020 (2000).

[20] X. Feng, M. Fehler, S. Brown, T. L. Szabo, and D. Burns, Short-period nonlinear viscoelastic memory of rocks revealed by copropagating longitudinal acoustic waves, J. Geophys. Res. Solid Earth **123**, 3993 (2018).

[21] M. Scalerandi, A. S. Gliozzi, C. L. E. Bruno, and P. Antonaci, Nonequilibrium and hysteresis in solids: Disentangling conditioning from nonlinear elasticity, Phys. Rev. B - Condens. Matter Mater. Phys. **81**, 104114 (2010).

[22] M. Scalerandi, M. Bentahar, and C. Mechri, Conditioning and elastic nonlinearity in concrete: Separation of damping and phase contributions, Constr. Build. Mater. **161**, 208 (2018).

[23] M. Wyrzykowski, A. M. Gajewicz-Jaromin, P. J. McDonald, D. J. Dunstan, K. L. Scrivener, and P. Lura, Water redistribution within the microstructure of cementitious materials due to temperature changes studied with 1H NMR, J. Phys. Chem. C **123**, 16153 (2017).

[24] J. A. Bittner and J. S. Popovics, Direct imaging of moisture effects during slow dynamic nonlinearity, Appl. Phys. Lett. **114**, 021901 (2019).

[25] P. Guéguen, P. A. Johnson, and P. Roux, Nonlinear dynamics induced in a structure by seismic and environmental loading, J. Acoust. Soc. Am. **140**, 582 (2016).

[26] M. W. Barsoum, A. Murugaiah, S. R. Kalidindi, and T. Zhen, Kinking Nonlinear Elastic Solids, Nanoindentations, and Geology, Phys. Rev. Lett. **92**, 255508 (2004).

[27] J. Jin, J. Rivière, Y. Ohara, and P. Shokouhi, Dynamic acousto-elastic response of single fatigue cracks with different microstructural features: An experimental investigation, J. Appl. Phys. **124**, 075303 (2018).

[28] R. Snieder, C. Sens-Schönfelder, and R. Wu, The time dependence of rock healing as a universal relaxation process, a tutorial, Geophys. J. Int. **208**, 1 (2017).

[29] M. Seifi, A. Salem, D. Satko, J. Shaffer, and J. J. Lewandowski, Defect distribution and microstructure heterogeneity effects on fracture resistance and fatigue behavior of EBM ti-6Al-4V, Int. J. Fatigue **94**, 263 (2017).

[30] A. H. Chern, P. Nandwana, R. McDaniels, R. R. Dehoff, P. K. Liaw, R. Tryon, and C. E. Duty, Build orientation, surface roughness, and scan path influence on the microstructure, mechanical properties, and flexural fatigue behavior of ti-6Al-4V fabricated by electron beam melting, Mater. Sci. Eng. A **772**, 138740 (2020).

[31] M. Zuo, M. Sokoluk, C. Cao, J. Yuan, S Zheng, and X. Li, Microstructure control and performance evolution of aluminum alloy 7075 by nano-treating, Sci. Rep. **9**, 10671 (2019).

[32] See Supplemental Material at http://link.aps.org/supplemental/10.1103/PhysRevApplied.17.014002 for additional details about experimental configuration and data analysis.

[33] M. Lott, C. Payan, V. Garnier, P. Y. Le Bas, T. J. Ulrich, and M. C. Remillieux, Three-dimensional modeling and numerical predictions of multimodal nonlinear behavior in damaged concrete blocks, J. Acoust. Soc. Am. **144**, 1154 (2018).

[34] C. Mechri, M. Scalerandi, and M. Bentahar, Separation of Damping and Velocity Strain Dependencies Using an Ultrasonic Monochromatic Excitation, Phys. Rev. Appl. **11**, 054050 (2019).

[35] P. Gueguen, M.-A. Brossault, P. Roux, and J.C. Singaucho, Slow dynamics process observed in civil engineering structures to detect structural heterogeneities, Eng. Structures **202**, 109833 (2020).

[36] J. Bergström, *Linear Viscoelasticity, in Mechanics of Solid Polymers* (Elsevier, Chadds Ford, PA, USA, 2015), 309.

[37] N. Pugno, F. Bosia, A. S. Gliozzi, P. P. Delsanto, and A. Carpinteri, Phenomenological approach to mechanical damage growth analysis, Phys. Rev. E **78**, 046103 (2008).

[38] B. Barzdajn, A. T. Paxton, D. Stewart, and F. P. E. Dunne, A crystal plasticity assessment of normally-loaded sliding contact in rough surfaces and galling, J. Mech. Phys. Solids **121**, 517 (2018).

[39] A. Di Bella, A. S. Gliozzi, M. Scalerandi, and M. Tortello, Analysis of elastic nonlinearity using continuous waves: Validation and applications, Appl. Sci. **9**, 5332 (2019).

[40] G. G. Kenning, D. L. Schlagel, and V. Thompson, Experimental determination of the critical spin-glass correlation length in single-crystal CuMn, Phys. Rev. B **102**, 064427 (2020).

[41] E. Pereiro-Lopez, W. Ludwig, and D. Bellet, Discontinuous penetration of liquid Ga into grain boundaries of Al polycrystals, Acta Mater. **52**, 321 (2004).

[42] E. Larose and S. Hall, Monitoring stress related velocity variation in concrete with a $2 \times 10^{-}5$ relative resolution using diffuse ultrasound, J. Acoust. Soc. Am. **125**, 1853 (2009).

[43] H. J. Lim and H. Sohn, Fatigue crack detection using structural nonlinearity reflected on linear ultrasonic features, J. Appl. Phys. **118**, 244902 (2015).

[44] G. Z. Chen, Y. X. Zhang, O. Abraham, D. Pageot, M. Chekroun, and V. Tournat, Numerical parametric study of nonlinear coda wave interferometry sensitivity to microcrack size in a multiple scattering medium, Ultrasonics **116**, 106483 (2021).

[45] A. Khanolkar, T. Yao, Z. Hua, C. A. Dennett, S. J. Reese, R. S. Schley, L. He, J. R. Kennedy, and D. H. Hurley, In situ monitoring of microstructure evolution during thermal processing of uranium-zirconium alloys using laser-generated ultrasound, J. Nucl. Mater. **553**, 153005 (2021).

[46] S. I. Rokhlin, G. Sha, J. Li, and A. L. Pilchak, Inversion methodology for ultrasonic characterization of polycrystals with clusters of preferentially oriented grains, Ultrasonics **115**, 106433 (2021).

[47] O. I. Lobkis and S. I. Rokhlin, Characterization of polycrystals with elongated duplex microstructure by inversion of ultrasonic backscattering data, Appl. Phys. Lett. **96**, 161905 (2010).

[48] I. K. Tragazikis, T. Z. Kordatou, D. A. Exarchos, P. T. Dalla, and T. E. Matikas, Monitoring the hydration process in carbon nanotube reinforced cement-based composites using nonlinear elastic waves, Appl. Sci. **11**, 1720 (2021).

[49] A. Astorga and P. Gueguen, Structural health building response induced by earthquakes: Material softening and recovery, Eng. Rep. **2**, e12228 (2020).

[50] M. Bentahar, A. Di Bella, C. Mechri, S. Montresor, M. Scalerandi, and X. Yu, Exploiting slow dynamics effects for damage detection in concrete, Front. in Built Environ. **6**, 64 (2020).

[51] J. Kober, A. Kruisova, and M. Scalerandi, Elastic slow dynamics in polycrystalline metal alloys, Appl. Sci. **11**, 8631 (2021).